Journal of VLSI Design Tools & Technology
Volume 1, Issue 1-3 Compilation 2011

STM JOURNALS

Modelling of Skin Effect in On-Chip VLSI RLC Global Interconnect

Vikas Maheshwari[1], Shilpi Lavania[1], Rajib Kar[2], Durbadal Mandal[2] & A. K. Bhattacharjee[2]*
[1]Department of ECE, Hindustan College of Science and Technology, Mathura, U.P., INDIA
[2]National Institute of Technology, Durgapur-9, West Bengal, INDIA

ABSTRACT

This paper addresses one of the aspects of the high frequency effects, namely the skin effect. The basic problem with skin effect is that it attenuates the high frequency components of a signal more than that of the low frequency components. Due to the increase in operating frequency and die sizes, RC models are becoming insufficient for analysis of global VLSI interconnects. Accurate noise modelling for RLC lines is thus critical for timing and signal integrity analysis. Skin effect basically affects the resistance and also the inductance, which in turn affects the system integrity in particular and its response as a whole. The current distribution inside the conductor changes as frequency increases. These changes produced in the conductors are known as skin and proximity effect. Till now the skin effect has been neglected for the modelling the on-chip interconnects. But with the increase in frequency to the GHz range, the skin effect has become prominent in performance parameter modelling. In this paper, firstly a crosstalk noise formula for on chip VLSI interconnects has been proposed without considering the skin effect. The voltage response at the output node is analytically derived and then the skin effect on the line resistance is analysed. From that an efficient and novel model is derived to estimate the crosstalk in the on-chip interconnects. On-chip inductive effects are becoming predominant in deep submicron interconnects due to increasing clock speeds; circuit complexity and decreasing interconnect lengths. Inductance causes noise in the signal waveforms, which can adversely affect the performance of the circuit and signal integrity. In this paper, we have also proposed a novel analytical model to find the impact of the skin effect on the noise in RLC interconnect without considering the skin effect on inductance because the value of the resistance increases dramatically compared to that of the value of inductance. In this work, the resistance variation due to the skin effect is considered in two wire transmission line model. The correlation between the skin effect and the noise induced is also discussed. The simulation results justify the efficacy of the proposed crosstalk noise model in the presence of skin effect.

Keywords: *On-Chip Interconnect, Skin- Effect, Crosstalk, RLC Segments, Coupling, VLSI*

Author for Correspondence E-mail: maheshwari_vikas1982@yahoo.com;
Tel: +919411403550

INTRODUCTION

Since late 80's, there have been a number of significant researches towards better and accurate modelling and characterization of the resistance, capacitance and the inductance of on-chip VLSI interconnect.

In recent years, increase in bandwidth requirements have led to the research into low-loss on-chip interconnects, which theoretically can achieve very high bandwidth [1]. For integrated circuits in the deep submicron (DSM) technology, interconnects play an important role in determining the chip performance and signal integrity. In deep submicron design, interconnect delay is shown to be ten to few hundred times larger than the intrinsic gate delay [2]. In order to reduce interconnect delay, wire-sizing is found to be an effective way. On-chip interconnect analysis begins with an in-depth coverage of delay metrics, including the ubiquitous Elmore delay [3] and its many variations. The study and analysis of

interconnect line has become very important issue because as integrated circuit feature sizes continue to scale well below 0.18µm, active device counts are reaching hundreds of millions [4]. The amount of interconnects among the devices tends to grow super linearly with the transistor counts, and the chip area is often limited by the physical interconnect area. Due to these interconnect area limitation, the interconnect dimensions are scaled with the devices whenever possible. Wire sizing [5] is found to be effective in reducing interconnect delays. Continuous wire sizing is a well suited approach which describes the wire by a continuous shape function. Studies on Elmore delay model have found that optimal shape function is exponential or near exponential. As frequency increases, current density within the conductor varies in such a way that it tends to exclude magnetic flux inside the conductor. This situation results in an apparent increase in resistance of the conductor because maximum current is concentrated near the surface and edges of the conductor, and it also causes the effective inductance of the conductor to decrease as frequency increases. These two effects become especially important when modelling the performance of high-speed data signals. Accurate prediction of propagation delay, crosstalk and pulse distortion in high-speed interconnects is strongly dependent on the per-unit parameters' model accuracy. For example, compared to a RLC model, the RC line model may generate an error of up to 30% of the total system [6]. There are a number of approaches available where the on-chip interconnect is modelled as distributed RLC segments for accurate performance parameters modelling [7–14]. But these models do not consider the high frequency skin effect phenomena.

Generally, in cases when high frequencies are considered, no insulator is perfect, and thus, there is always a probability of leakage, and conductance is considered as a measure of this leakage. Despite the technological impact of the skin effect, published models are mostly limited to traditional wire structures such as coaxial cables [15–16]. For on-chip and on-board applications, it is important to estimate the effect for single wires rather than complete transmission lines with a rectangular rather than circular cross-section. Skin effect and the change in inductance are inextricably linked. A SPICE model also links these two effects [17]. The simplest model for an incremental length of transmission line is the basic series inductance L_1 and a lossless shunt capacitance C, with some resistor R_1 in series with the inductance as shown in Figure 1. R_1 can be either fixed or frequency-dependent to account for skin-effect losses. However, this simple model has no provision to change the signal velocity. In another model, part of the series inductance has a shunt resistance across it and is shown in Figure 2. Note that, at low frequencies, the total inductance is simply the sum of L_1 and L_2, and the loss due to shunt resistor R_2 is negligible because its impedance is much higher than that of L_2. As frequency

increases, R_2 becomes dominant and causes more losses as the impedance of L_2 increases.

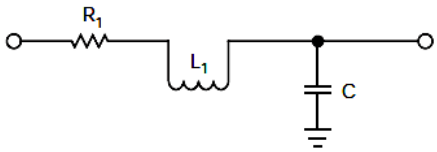

Fig. 1: Simple RLC Model

Thus, L_2 and R_2 perform the same function that occurs in a conductor, i.e., as current inside the conductor excludes some of the internal magnetic-flux lines, the apparent inductance decreases, and the loss increases. By changing the values of L_1, L_2, R_1 and R_2, this simple circuit can model the resistance and inductance of an actual conductor.

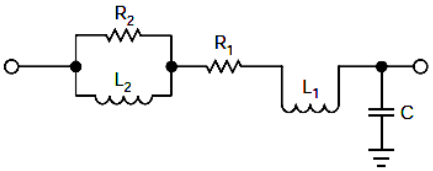

Fig. 2 Another type of RLC Model

This paper presents an analytical method for the crosstalk aware delay estimation of on-chip VLSI interconnects due to the high frequency of operation where the skin effect has been considered.

The rest of the paper is organized as follows: Basic theory, regarding the previous works and researches are discussed in section 2. Section 3 describes the proposed model for the delay for different type of poles. Simulation results are shown in Section 4, while Section 5 concludes the paper.

BASIC THEORY

The skin effect can be represented at the circuit level as a combination of frequency-dependent resistance and inductance. However, frequency-dependent circuit elements are not suitable for time-domain analysis. Therefore, a circuit representation based on frequency-independent elements is desirable. All circuit models presented in the literatures are based on the ladder topology as shown in Figure-3 or the parallel topology as Figure-4. In both cases, the external inductance L_{ext} is frequency-independent, while the internal impedance (resistance and inductance) is modelled by a combination of resistors and inductors. The external inductance coincides with the asymptotic value of inductance at high frequencies and corresponds to the limit where all current flows on the wire surface and no fields exist inside the wire:

$L_{ext} = L_{hf}$

The internal inductance [18] is the difference between the low- and high-frequency limits:

$L_{int} = L_{lf} - L_{hf}$; where L_{lf}, L_{hf} are the inductance at low and high frequency, respectively.

This is due to field penetration inside the conductor. Typically, internal inductance accounts for less than 10% of the total low frequency (partial) inductance of a single wire, or open loop [18]. For closely spaced loops, due to cancellation of the self and mutual inductances, the internal inductance can be a significant portion of the loop inductance.

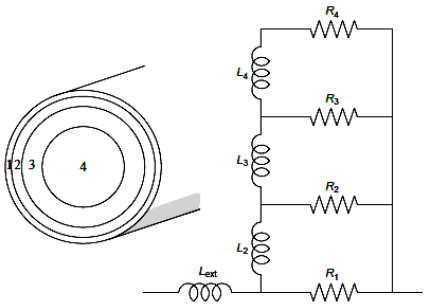

Fig. 3 Ladder Topology for Skin Effect

The ladder topology as shown in Figure-3 has been introduced by Wheeler *et al.* [26] and developed by Yen et al. [19] and Kim and Neikirk [20]. This topology can be rigorously justified from Maxwell's equations in the quasi-static limit, where each resistor R_i corresponds to a concentric shell in the physical conductor. Exact expressions for the inductances in the case of a circular cross section can be computed for a very fine discretization, i.e., a large number of thin shells [20]. However, no accurate expressions for the L_i's are known for a noncircular cross section, or a small number of shells. Kim and Neikirk [20] developed a technique based on the ad-hoc assumption of a geometric progression of the resistance and inductance values:

$$R_{i+1} = \frac{R_i}{RR}, L_{i+1} = \frac{LL}{L_i} \quad (1)$$

Once R_1 and L_2 are empirically set, the ratios RR and LL are chosen to satisfy constraints on the low frequency resistance R and internal inductance L_{int}. The free parameters in the model are,

$$\alpha_R = \frac{R_1}{R}, \alpha_L = \frac{L_{\text{int}}}{L_2} \quad (2)$$

In [20], empirical rules were given to compute α_R and α_L based on wire radius and maximum frequency of operation. These are empirically fitted to exact analytical results or measurements. The fit was performed for a few representative cases; however, no accounting for non-circular geometries was given. Also, estimations of L_{ext} and L_{int} are not discussed except for some special cases.

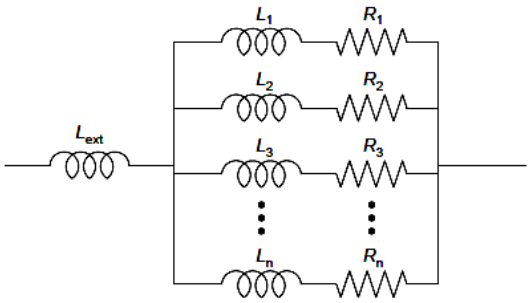

Fig. 4 Parallel Topology for Skin-Effect

The parallel *RL* topology, as shown in Figure-4 has no direct physical interpretation. However, due to its simplicity, it is well suited for empirical fit of its parameters to measure data or exact theoretical results. Sen and Wheeler et. al. [21] proposed a set of rules to determine the parameters R_i and L_i for arbitrary number of parallel branches. Their derivation is similar to that of [20] as both are based on the arbitrary assumption of the geometric scaling of the resistors and inductors and the conservation of R and L_{int}. Also in this case, no estimate was given for L_{ext} and L_{int}. Mei and Ismail [15] used the parallel *RL* topology as a template for the model reduction of a complete, filament-based calculation. However, the model generation requires extensive calculations and no compact expressions are given.

In order to assess the efficacy of published models, we need to find a way to obtain the internal inductance of a wire for a given geometry, without relying on numerical solvers. However, the only formula readily available to estimate internal inductance is valid for a wire with circular cross section and is given in (3).

$$L_{\text{int}} = \frac{\mu l}{8\pi} \tag{3}$$

Choudhury *et al*. [22] considered the internal inductance of a rectangular wire, however, no expressions were provided for a generic aspect ratio. A satisfactory fit [22] for a wire with width *W* and height *H* is given by the expression (4).

$$L_{\text{int}} = 10^{-9} l \left[0.3 + 0.28 e\left(-0.14 \frac{W}{H} \right) \right] \tag{4}$$

Where, the wire length *l* is in centimetres, and *W* >*H* (the ratio *H/W* should be substituted for *W/H* in the opposite case). It has been verified the accuracy of this expression by comparison with results obtained from Fast Henry [22]. To ensure an accurate numerical modelling, a 20×20 filament matrix has been adopted in the Fast Henry simulations. Note that Fast Henry performs a magneto static calculation, where couplings along the wire length are fully accounted for. The normalized internal inductance is essentially independent of length, but is strongly dependent on the wire aspect ratio. As explained in the next section, we will use this scalability to construct a model where all frequency-dependent quantities are independent of length. The figure also compares the analytical fit to (4). Figure 5 shows the comparison between values of resistance and inductance obtained from Fast Henry [4] and the model of Sen and Wheeler [21]. This work considered the case of copper wires, of length 1 mm, with rectangular cross sections of constant area ($100\mu m^2$) and aspect ratios of 1, 4, and 16. As discussed above, the use of (4) allows a good fit of the inductance curve. However, the most dramatic consequence of the skin effect is not observed on the inductance, but on the resistance, which increases by over a factor of 10 from dc to 100 GHz. Since the wire geometry is not explicitly accounted for in the model, the qualitative dependence of resistance on the aspect ratio is captured only incidentally, and the quantitative match is not satisfactory, with errors exceeding 20%. A similar result is obtained from the ladder model of Kim and Neikirk [20]. Also in this case, (4) can be used to separate the internal from the external inductance. Since the original model was fitted on nonrectangular cross-sections, we recalibrated it from numerical simulations. Using least-squares optimization, we determined the parameters α_R and α_L for a wide range of aspect ratios. Figure 6 shows the result of the fit for the same aspect ratios of Figure 5. Also here, an error exceeding 20% is observed for the case *W/H* = 16. The slope of the R (f) curve for high aspect ratios is quite lower than for the Kim-Neikirk

model, and the best fit crosses the numerical value rather than following it.

Note the since an exhaustive optimization procedure was followed, no choice of model parameter exists that gives a better result. In fact, the assumption of fixed element scaling limits the representational power of the model. Moreover, the model parameters (α_R and α_L) do not have an immediate physical interpretation, and their scaling with the wire geometry is not obvious.

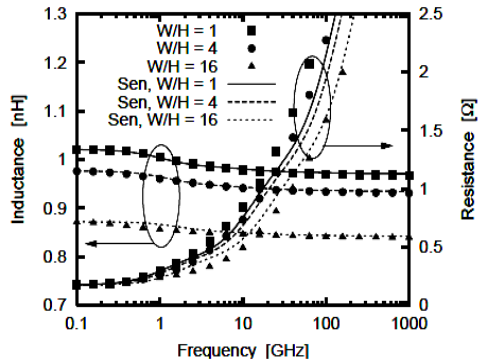

Fig. 5 Comparison between Fast Henry results (symbols) and the parallel-RL equivalent circuit of Sen and Wheeler [21] (lines).

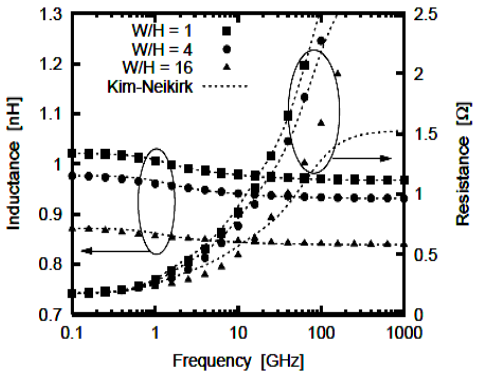

Fig. 6 Comparison between Fast Henry results (symbols) and the ladder model of Kim and Neikirk [20] (dashed lines).

PROPOSED WORK

The proposed work is divided in two sub-sections. In the first sub-section, a novel analytical crosstalk model of RLC interconnect is proposed which does not included the skin effect; whereas, in the second sub-section, the skin effect is considered for RLC interconnect modelling. Note that the skin effect makes an adverse effect on the resistance and the inductance. However, this paper only considered the skin effect onto the resistance. The resistance increases with the skin effect; whereas, a decrease in the inductance is accounted.

Crosstalk Modelling of RLC Interconnect Analysis Without Skin Effect

In this section a new analytical model of RLC interconnects is proposed. This analysis considers the following interconnect coupling circuit:

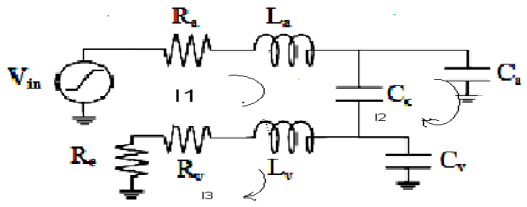

Fig. 7: Analytical Model of RLC interconnect.

Now applying the simple loop analysis, the following equations are obtained in terms of RLC:

For first loop:

$$V_{in}(t) = I_1(t).R_a + L_a.\left(\frac{d}{dt}I_1(t)\right) + \frac{1}{C_c}[I_1(t) - I_2(t)] \quad (5)$$

(15)

For second loop:

$$\frac{1}{C_c}[I_2(t)-I_1(t)]-\frac{1}{C_a}I_2(t)=0 \qquad (6)$$

For third loop:

$$R_e I_3(t)+R_v\cdot I_3(t)+L_v\cdot\frac{d}{dt}(I_3(t))+\frac{1}{C_c}\cdot I_3(t)=0 \qquad (7)$$

Taking Laplace Transform of (5) - (7), the following equations are obtained:

$$V_{in}(s)=I_1(s)R_a+sL_aI_1(s)+\frac{[I_1(s)-I_2(s)]}{sC_c} \qquad (8)$$

$$\frac{1}{sC_c}[I_2(s)-I_1(s)]-\frac{1}{sC_a}I_2(s)=0 \qquad (9)$$

$$R_eL_3(s)+R_vI_3(s)+sL_vI_3(s)+\frac{1}{sC_v}.I_3(s)=0 \qquad (10)$$

From (9), the following can be derived:

$$\left[\frac{1}{sC_c}-\frac{1}{sC_a}\right]I_2(s)=\frac{1}{sC_c}I_1(s) \qquad (11)$$

Or, $$I_2(s)=\frac{I_1(s)}{sC_c\left(\frac{1}{sC_c}-\frac{1}{sC_a}\right)} \qquad (12)$$

So, $$I_2(s)=I_1(s)\left(\frac{C_a}{C_a-C_c}\right) \qquad (13)$$

From equation (8),

$$V_{in}(s)=I_1(s).R_a+sL_aI_1(s)+\frac{1}{C_c}I_1(s)-\frac{1}{C_c}I_1(s).\frac{C_a}{C_a-C_c} \qquad (14)$$

Or,

$$V_{in}(s)=I_1(s)\left[R_a+sL_a+\frac{1}{C_c}\left(1-\frac{C_a}{C_a-C_c}\right)\right]$$

So, $$I_1(s)=\frac{V_{in}(s)}{R_a+sL_a+\frac{1}{C_c}\left(1-\frac{C_a}{C_a-C_c}\right)} \qquad (16)$$

With the simple loop analysis it can be found that

$$I_3=|I_1-I_2| \qquad (17)$$

Therefore, using I_1 and I_2, the third current can be derived which is given as,

$$I_3(s)=\frac{V_{in}(s)C_c}{R_a+sL_a+\frac{1}{C_c}\left(1-\frac{C_a}{C_a-C_c}\right)(C_a-C_c)} \qquad (18)$$

Applying the current divider rule, the current in the victim line capacitor may be found. This finally yields to,

$$I_x=I_3\frac{R_2}{R_1+R_2} \qquad (19)$$

where $R_1=(R_e+R_v+sL_v)or,R_1=\frac{1}{sC_v}$

$$I_x=\frac{V_{in}(s)C_c}{R_a+sL_a+\frac{1}{C_c}\left(1-\frac{C_a}{C_a-C_c}\right)(C_a-C_c)}\times\frac{R_e+R_v+sL_v}{R_e+R_v+sL_v+\frac{1}{sC_v}} \qquad (20)$$

The output voltage is given as,

$$V_{co}(s)=I_x\times\frac{1}{sC_v} \qquad (21)$$

From (20) and (21) we have,

$$V_{co}(s)=\frac{V_{in}(s)}{sC_v}\left[\frac{C_c(R_e+R_v+sL_v)}{\left(R_a+sL_a+\frac{1}{C_c\left(1-\frac{C_a}{C_a-C_c}\right)}\right)\left(R_e+R_v+s\left(L_v+\frac{1}{s.sC_v}\right)\right)\times(C_a-C_c)}\right] \qquad (22)$$

Some important assumptions that have been made in this paper are as follows:

$$R_e + R_v = A$$

$$R_a + \frac{1}{C_c}\left[1 - \frac{C_a}{C_a - C_c}\right] = B \qquad (23)$$

For step input, $V_{in} = \frac{V_0}{s}$ (24)

Using the above assumptions and applying partial fraction theory yields,

$$V_{co}(s) = \frac{V_0}{s^2(C_a - C_c)}\left[\frac{C_c(A + sL_v)}{(B + sL_a)\times(1 + A + sL_v)}\right] \qquad (25)$$

$$S(s) = \frac{F_1}{s} + \frac{F_2}{s^2} + \frac{F_3}{(B + sL_a)} + \frac{F_4}{(1 + A + sL_v)} \qquad (26)$$

$$F_1 = \frac{d}{ds}(S(s).s^2)|_{s=0} =$$
$$\frac{d}{ds}\left[\frac{C_c(A + sL_v)}{(B + sL_a)(1 + A + sL_v)}\right]|_{s=0}$$
$$= \frac{B(A+1)C_cL_v - C_c.A(B.L_v + L_a(A+1))}{\left[B(A+1)^2\right]} \qquad (27)$$

$$F_2 = S(s).s^2|_{s=0} =$$
$$\left(\frac{C_c(A + sL_v)}{(1 + A + sL_v)(B + sL_a)s^2}\right).s^2|_{s=0} = \frac{C_cA}{B(A+1)} \qquad (28)$$

$$F_3 = S(s)(B + sL_a)|_{s=-\frac{B}{L_a}} = \frac{C_c(A + sL_v)}{(1 + A + sL_v)s^2}|_{s=-\frac{B}{L_a}}$$
$$= \frac{C_c\left(A - \frac{B}{L_a}L_v\right)}{\left[(A+1) - \frac{B}{L_a}L_v\right]\left(-\frac{B}{L_a}\right)^2} \qquad (29)$$

$$F_4 = S(s)(1 + A + sL_v)|_{s=-\frac{A+1}{L_v}}$$
$$= \frac{C_c(A + sL_v)}{s^2(B + sL_a)}|_{s=-\frac{(A+1)}{L_v}}$$
$$= -\frac{C_c}{\left[B - (A+1)\frac{L_a}{L_v}\right]\left(\frac{1+A}{L_v}\right)^2} \qquad (30)$$

Taking the Laplace inverse transforms of (25) and with the help of (26)-(30), one can derive the explicit expression for $V_{co}(t)$ and it is given in (31).

$$V_{co}(t) = \frac{V}{(C_a - C_c)_0}\left[\begin{array}{l}\left(\frac{B(A+1)C_cL_v - C_cA(BL_v + L_a(A+1))}{[B(1+A)]^2}\right)u(t) \\ + \frac{C_cA}{B(1+A)}.t.u(t) + \\ \frac{C_c\left(A - \frac{B}{L_a}L_v\right)}{\left[(A+1) - \frac{B}{L_a}L_v\right]\left(-\frac{B}{L_a}\right)}e^{-\frac{B}{L_a}t} \\ - \frac{C_c}{\left[B - (1+A)\frac{L_a}{L_v}\right]\left[\frac{A+1}{L_v}\right]^2}e^{-\frac{(1+A)}{L_v}t}\end{array}\right] \qquad (31)$$

The equation (31) describes the coupling noise voltage without the presence of skin effect phenomena.

Crosstalk Modeling of RLC Interconnect With Skin Effect

In this section, we have considered the performance variations of interconnect due to the presence of the skin effect phenomena. The skin effect is the tendency of high frequency current density to be highest at the surface of a conductor and then to decay exponentially towards the centre [23].

The possible reasons for which one must care the skin effect are the following:

The resistance of a conductor is inversely proportional to the cross sectional area of the conductor. If the cross sectional area decreases, the resistance goes up. The skin effect causes the effective cross sectional area to decrease. Therefore, the skin effect causes the effective resistance of the conductor to increase [24].

The skin effect is a function of frequency. Therefore, the skin effect causes the resistance of a conductor to become the function of frequency. This, in turn, affects the impedance of the conductor. The inductance decreases as the frequency increases [24]. It is simple to analyze the skin effect in a homogeneous conducting half space with the current parallel to the interface. Let the current is in z-direction and y axis is normal to the interface as shown in the Figure 8.

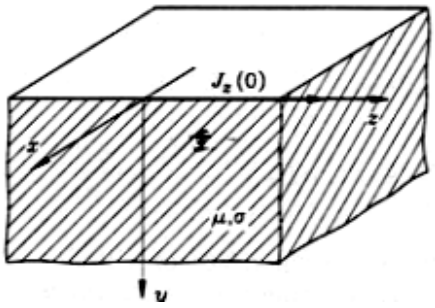

Fig. 8 Homogeneous Conducting Half Space.

If the angular frequency of the current is ω, and the medium has a conductivity σ, and permeability μ, the complex current density is found to be:

$$J_z(y) = J_z(0).e^{-ky}e^{-jky} \qquad (32)$$

where, $k = \sqrt{\frac{\omega\sigma\mu}{2}}$

The intensity of the current density vector decrease exponentially with increasing y. At a distance δ,

$$\delta = \frac{1}{k} = \sqrt{\frac{2}{\omega\mu\sigma}} \qquad (33)$$

The amplitude of the current density vector decreases 1/e of its value $J_z(0)$ at the boundary surface. This distance is known as the "skin depth". In Table-1, the skin depths of various materials are shown.

Skin depth for Copper is $\sigma = 57\times10^6 S/m, \mu = \mu_0$, for iron $\sigma = 10^7 S/m, \mu_r = 1000$, for sea water $\sigma = 4S/m, \mu = \mu_0$, for wet soil $\sigma = 0.01S/m, \mu = \mu_0$.

TABLE I KIN DEPTH FOR VARIOUS MATERIALS

Material	f = 60Hz	f = 10^3Hz	f =10^6Hz	F =10^9Hz
Copper	8.61 mm	2.1 mm	.067 mm	2.11 μm
Iron	0.65 mm	0.16 mm	5.03 μm	0.016 μm
Sea Water	32.5 m	7.96 m	.25 m	7.96 μm
Wet Soil	650 m	159 m	5.03 m	0.16 μm

It is mentioned earlier that we have only considered the skin effect on resistance. So for calculating the total effect on the impedance we have to calculate the output impedance.

From the Figure 7,

$$Z_1 = \frac{\left[R_v + R_e + sL_v\right] \times \frac{1}{sC_v}}{(R_v + R_e + sL_v) + \frac{1}{sC_v}} \quad (34)$$

$$Z_2 = \frac{(R_v + R_e + sL_v) \times \frac{1}{sC_v}}{(R_v + R_e + sL_v)} + \frac{1}{sC_c} \quad (35)$$

$$Z_3 = \left\{ \frac{\left[\frac{\left[R_v + R_e + sL_v\right] \times \frac{1}{sC_v}}{\left[R_v + R_e + sL_v + \frac{1}{sC_v}\right]} + \frac{1}{sC_c} \right] \times \frac{1}{sC_a}}{\frac{(R + R + sL) \times \frac{1}{sC}}{(R_v + R_e + sL_v) + \frac{1}{sC_v}} + \frac{1}{sC_c} + \frac{1}{sC_a}} \right\} \quad (36)$$

The total output resistance in RLC interconnects is given in (37)

$$Z_0 = \left[\frac{\left(\frac{(R + R + sL) \times \frac{1}{sC_v}}{(R_v + R_e + sL_v) + \frac{1}{sC_v}} \right) \times \frac{1}{sC_a}}{(R_v + R_e + sL_v) \times \frac{1}{sC_v} + \frac{1}{sC_c} + \frac{1}{sC_a}} \right] + (R_a + sL_a) \quad (37)$$

Skin effect on resistance can be calculated by using the following equations:

$$R_{total} = R_{DC} + \sqrt{f} R_{AC}, \quad (38)$$

Where, $R_{DC} = \frac{\rho L}{W.t}$ (39)

$$R_{AC} = \frac{\rho L}{A_{current\_densityar\_area}} = \frac{L\rho}{\omega\sqrt{\frac{2}{\omega\sigma\mu}}} = \frac{L\sqrt{\rho}}{\omega\sqrt{2}}\sqrt{\mu f} \quad (40)$$

Therefore,

$$R = R_{total} = \frac{\rho L}{Wt} + \frac{L\sqrt{\rho}}{\omega\sqrt{2}} \cdot \sqrt{\mu f} \quad (41)$$

It is evident from the above equation that resistance increases as a function of the

square root of the frequency due to the skin effect.

The skin depth can be calculated as:

$$\delta = \sqrt{\frac{2\rho}{2\Pi f \mu_r \mu_0}} m$$

SIMULATION RESULT

The motive of this paper is to make a reflection on the skin effect impact on the on chip interconnect and its performance. It can be analyzed by the simulation result that the delay has been increased. This is due to the fact that skin effect has an adverse effect on the resistance, so, with the existence of the skin effect the resistance is increased as discussed in the section 2. This increase in the resistance in turn increases the delay which is undesirable in terms of speed of the chip. The configuration of circuit for simulation is shown in Figure7. We now develop a simple model for distributed RLC interconnect line. The high-speed interconnect system consist of two coupled interconnect lines and ground and the length of the lines is d =100 um. These lines are excited by the voltage source of 1.8 V with driver resistance of R_s. The extracted values for the parameters R, L, and C are given in Table 2 [27]. We compare the delays obtained from SPICE with those proposed model in both the cases i.e. with and without considering the skin effect on the interconnect lines. Table 3 and

Table 4 compare the delay obtained from SPICE with those found using the proposed model without and with considering skin effect. Note that the difference between the proposed model and the SPICE delay is about 1% in both the cases. Figures 9 and 10, respectively, show the response of the system with and without considering skin effect, respectively. From these figures we can analyse that the resistance of the interconnect line increases from 120 kΩ to 1560 kΩ due to skin effect. Figure (11) and (12) demonstrate the behaviour of output node noise voltage curve with and without considering the skin effect respectively.

TABLE II RLC PARAMETERS FOR A MINIMUM-SIZED WIRES IN A 0.18μM TECHNOLOGY.

Parameter(s)	Value/m
Resistance(R)	120 kΩ/m
Inductance(L)	270 nH/m
Capacitance(C)	240 pF/m
Coupling Capacitance(C_c)	682.49 fF/m

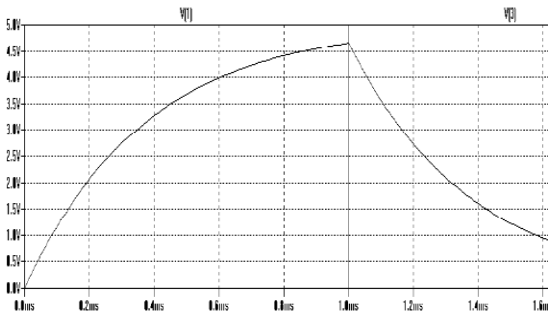

Fig. 9: Response of the proposed model with considering Skin Effect R=1560 KΩ.

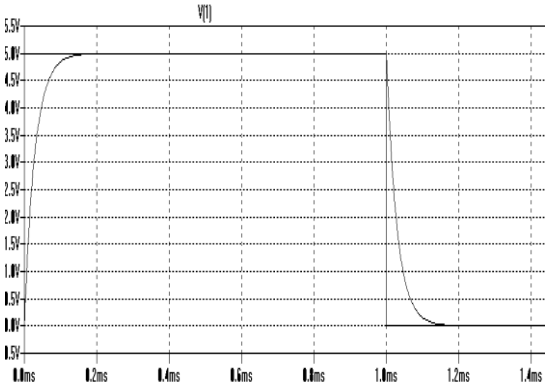

Fig. 10: Response of the Proposed model without considering Skin Effect for R=120 KΩ.

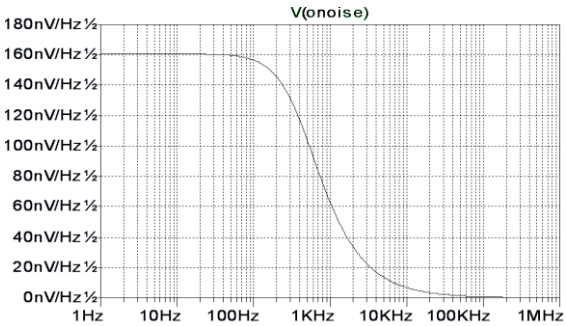

Fig. 11: Output node noise with considering skin effect for R=1560 KΩ.

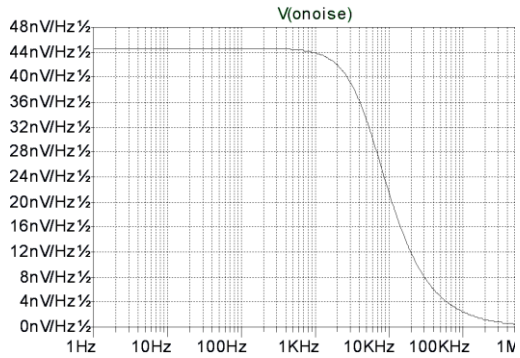

Fig. 12 Output node noise without considering skin effect for R=120 KΩ.

TABLE III EXPERIMENTAL RESULT UNDER STEP INPUT WITHOUT SKIN EFFECT

Ex	R_s (KΩ)	C_L (fF)	SPICE Delay (ms)	Proposed Model Delay (ms)
1	1	10	0.1023	0.1041
2	5	50	0.1124	0.1147
3	10	750	0.1393	0.1491
4	50	1000	0.1679	0.1779
5	100	1500	0.19595	0.1986

TABLE IV EXPERIMENTAL RESULT UNDER INPUT WITH SKIN EFFECT

Ex	R_s (KΩ)	C_L (fF)	SPICE Delay (ms)	Proposed Model Delay (ms)
1	1	10	0.1893	0.1904
2	5	50	0.4524	0.5167
3	10	750	0.7993	0.8191
4	50	1000	0.8699	0.8879
5	100	1500	0.9595	0.9986

The simulation shows that failure to account for the skin effect leads to three different errors. First, since the internal inductance is included in the line parameters, the line delay is overestimated. This error could be removed by including only the external inductance in the RLC model, but this would underestimate the inductive effect at low frequencies. Second, the attenuation suffered by the signal due to line resistance is underestimated. Finally, the higher inductance leads to a higher characteristic impedance and incorrectly predicts loss of matching at the input.

CONCLUSIONS

We proposed a new methodology for skin effect equivalent circuits, based on the fitting of the transfer function to numerical simulations. It is shown that the methodology allows arbitrary accuracy in the modelling of the skin effect, and can be adapted to different situations and modelling requirements. We propose a method for the calculation for the skin effect of RLC interconnects. It is shown that skin effect can be computed efficiently in the s-domain using an algebraic formulation, instead of the improper integration in the time domain. The proposed method of computing skin effect relies on the poles and residues of the transfer function and can be used in any kind of model order reduction technique. Compact expressions that describe the skin effect on a single distributed RLC interconnect are rigorously derived. The derived expression along with the analysis can serve as a convenient tool for skin effect without much computation during design. In this paper, we have also proposed a novel analytical model to find the impact of the skin effect on the noise in RLC interconnect without considering the skin effect on inductance because the value of the resistance increases dramatically with compare to the value of inductance. Simulation results demonstrate the validity and correctness of our proposed model.

REFERENCES

1. Kleveland B., Diaz C., Vook D. et al. *IEEE Journal of Solid-State Circuits* Oct., 2001. 36(10) 1480–1488p.
2. Celik M., Pileggi L. & Odabasioglu A. by Kluwer Academic Publishers. 2002.
3. Elmore W. C *Journal of Applied Physics* Jan., 1948.19(1) 55 – 63p.
4. Shien-Yang Wu, Boon-Khim Liew, Young K. L. et al. *Analysis of Interconnect Delay for 0.18µm Technology and Beyond* Interconnect Technology, IEEE International Conference 1999. 68 – 70p.
5. Magdy A. El-Moursy & Eby G. Friedman. *Integration, the VLSI Journal* 2004. 38. 205–225p.
6. Ismail Y. I. & Friedman E. G. *Effects of inductance on the propagation delay and repeater insertion in VLSI circuits* IEEE Transactions on Very Large Scale Integration (VLSI) Systems. Apr., 2000. 8(2) 195-206p.
7. Rajib Kar, V. Maheshwari, Aman Choudhary. et al. *International Journal of Signal & Image Processing (IJSIP)* ACEEE, USA. 2010. 1(2) 14-19p.
8. Madhumanti Datta, Susmita Sahoo, Debjit Ghosh. et al. *International Journal of VLSI Design, International Sciences Press* India. 2011. 2(1) 83-89p.
9. Susmita Sahoo, Madhumanti Datta, & Rajib Kar. *International Journal of Electrical and Electronics Engineering* WASET Publication. 2011. 5(3) 165–172p.
10. Susmita Sahoo, Madhumanti Datta, & Rajib Kar. et al. *Journal of Electronic Devices* France. 2011.10. 464–470p.
11. Madhumanti Datta, Susmita Sahoo, Debjit Ghosh et al. *An Accurate Analytical Crosstalk Model for On-Chip VLSI RLC Interconnect* International Conference on Communication and Signal Processing (ICCOS'11) Coimbatore, India. March 17–18, 2011. 1133–1137p.
12. Susmita Sahoo, Madhumanti Datta, & Rajib Kar. *An Explicit Delay Model for On-Chip VLSI RLC Interconnect* IEEE International Conference on Devices and Communications (ICDeCom-11) BIT Mesra, India. Feb 24-25, 2011. 1–6p.
13. Susmita Sahoo, Madhumanti Datta, & Rajib Kar. *An Efficient Dynamic Power Estimation Method for On-Chip VLSI Interconnects* 2nd IEEE International Conference on Emerging Applications of Information Technology (EAIT 2011) Kolkata, India. February 19-20, 2011. 379–382p.
14. Susmita Sahoo, Madhumanti Datta, & Rajib Kar. *An Explicit Delay Analysis of RLC Interconnect using Diffusion Equation Model* International Conference on Computational Vision and Robotics (ICCVR-2010) 21–22nd August, 2010. 206-213p.
15. Shizhong Mei, Chirayu Amin & Yehea I. Ismail. *Efficient Model Order Reduction*

Including Skin Effect DAC 2003 Anaheim, California, USA. 232–237p.

16. Wigington R. L. & Nahman N. S. *Transient Analysis of Coaxial Cables Considering Skin Effect* Proceedings of the IRE Feb, 1957. 45(2).166-174p.
17. Reference Data for Radio Engineers. Fifth Edition, Howard W Sams and Co. 1968.
18. Mukherjee B., Lei Wang & Pacelli A. *A Practical Approach to Modeling Skin Effectin On-Chip Interconnects* GLSVLSI'04, Boston, Massachusetts, USA. April 26–28, 2004.
19. Yen C.-S., Fazarinc Z. & Wheeler R. L. *Time-domain skin-effect model for transient analysis of lossy transmission lines* Proceedings of the IEEE. July, 1982. 70(7) 750–757p.
20. Kim S. & Neikirk D. P. *Compact equivalent circuit model for the skin effect* in IEEE International Microwave Symposium Digest. 1996, 1815–1818p.

    Sen B. & Wheeler R. L. *Skin effects models for transmission line structures using generic SPICE circuit simulators* IEEE Topical Meeting on Electrical Performance of Electronic Packaging. 1998. 128–131p.
21. Choudhury J., Seetharaman G. S. & G. H. Massiha *Accurate modelling of thin-film inductance for nano-chip* in Third IEEE Conference on Nanotechnology. 2003. 351–355p.
22. Skin Effect Douglas Brooks, Ultra-cad Design, Inc. http://www.ultracad.com
23. By CECIL DEISCH.TELLABS INC Modeling Skin effect in Spice Ultracad Designing.
24. Mei S. & Ismail Y. I. *Modelling skin effect with reduced decoupled R−L circuits* in Proceedings IEEE International Symposium on Circuit and Systems (ISCAS) 2003. 588–591p.
25. Wheeler H. A Proceedings of the IRE. Sept., 1942. 30. 412–424p.
26. Charlet F., Bermond C. & Putot S. et al. *Extraction of (R,L,C,G) interconnect parameters in 2D*

    transmission lines using fast and efficient numerical tools International Conference on Simulation of Semiconductor Processes and Devices (SISPAD) 2000. 87–89p.

